Numerical studies of the interstellar medium on galactic scales

Pelupessy, F.I.

Chapter 3

Feedback in SPH simulations of galaxies

Abstract

We examine two new methods for including supernova and stellar wind feedback in smoothed particle hydrodynamics (SPH) simulations of galaxies. The first method is based upon the return of energy as random motions in the gas. The second is based on the equations of motion of an ordinary SPH particle in the zero mass limit: we construct a separate type of particle, which we will call a *pressure particle*, associated with young stellar clusters, that acts on the gas through these equations. We check that both these methods give equivalent solutions to the problem of energy injection in gaseous media, compared with direct heating of the gas. We furthermore show that these methods circumvent the problems of conventional feedback implementations in simulations including the cooling of the ISM and star formation. We also examine the relation between HI properties and star formation, showing that our model reproduces observed correlations.

3.1 Introduction

Probably the greatest source of uncertainty in the theory of galaxy formation and evolution is the injection of mechanical energy into the interstellar medium (ISM) by young stellar clusters. Hybrid hydrodynamics/ N-body codes have proved to be useful tools to get a grip on the complexity of gravitational dynamics and ISM physics. An important source of heating that needs to be included in simulations is the mechanical luminosity of stellar clusters, which is the collective result of stellar winds and successive supernovae (SNe) explosions of massive stars in approximately the first 30 Myr of the lifetime of a cluster. For a cluster of given age and initial mass function (IMF) this mechanical luminosity can be determined from current stellar evolution models (e.g.. Starburst99 models, Leitherer et al. 1999), which incorporate the most recent results of stellar evolution theory and dynamic atmosphere modelling. In principle it is then not difficult to account for this as an extra term in the thermal evolution equations of a hydrodynamic simulation of the ISM.

However as was first observed by Katz (1992) in smoothed particle hydrodynamics (SPH, Gingold & Monaghan 1977, Lucy 1977, Monaghan 1992) simulations of galaxy formation, this naive implementation of supernova feedback will have little effect on the dynamics of the ISM. The reason for this is that a realistic model for the ISM must take into account cooling of the gas. The heating from the mechanical luminosity is small compared with the potential for cooling if, as in practice is always the case, the resolution of the ISM simulation is limited. We can write the heating $\Gamma_{\rm sn}$ due to a young star cluster that returns its energy to a nearby gas particle or gas cell, as $\Gamma_{\rm sn} = \mathbb{L}_{\rm mech}\frac{\rm M_{star}}{\rm M_{gas}}$, with $\mathbb{L}_{\rm mech}$ the mechanical luminosity of the young stellar cluster per unit mass of stars formed, $\rm M_{star}$ the mass of the star particle and $\rm M_{gas}$ the mass of the gas particle that receives the SN energy. For values $\mathbb{L}_{\rm mech} = 5$ erg g^{-1} s^{-1} (assuming 0.01 supernova of 10^{51} erg $\rm M_\odot{}^{-1}$ of stars formed and an active period of 30 Myr, which is approximately the the mechanical energy luminosity for a Salpeter IMF with mass boundaries 0.1 $\rm M_\odot$ and 100 $\rm M_\odot$) and $\rm M_{star}/M_{gas}$ of order unity (appropriate for current star formation recipes) we then get a heating of $\Gamma_{\rm sn} = 5$ erg g^{-1} s^{-1}, which is much smaller than the cooling Λ at the peak of the cooling curve at about 10^5 K of $\Lambda \approx 400$ $\rm n_H$ erg g^{-1} s^{-1}, for H densities $\rm n_H \gtrsim 1$ cm^{-3}. So returning the energy to the gas as heating will not result in temperatures higher than 10^5 K and usually much lower, and this is too small to alter the dynamics of the gas substantially. This is unrealistic: in practice hot gas will carve out a low density bubble where cooling is inefficient. Radiative losses are important, but occur in dense shells around this bubble. The problem of feedback implementation is not exclusive to SPH codes, it occurs also in other types of hydrodynamic codes, e.g. Eulerian grid codes (Fragile et al. 2003).

Note that increasing the resolution of the simulation alone will not solve the problem of radiative energy losses: increasing the resolution but keeping $\rm M_{star}/M_{gas}$ fixed, one will encounter the same problem. Only increasing the ratio $\rm M_{star}/M_{gas}$ to values $\gg 100$ would mitigate the problem, as this would allow the gas to attain a high temperature. This is normally the case in more detailed simulations of superbubbles (e.g. Mac Low & Ferrara 1999) due to starbursts. This is not practical in SPH simulations of galaxies that include star formation, because star formation in these simulations is sub-grid physics. Forming large star particles would impose graininess on the star formation rate. Furthermore, current methods of star formation use a local star formation method that changes a fraction of order unity of a gas particle's mass into stars conditional upon a criterion that depends on the thermodynamic state of that particle.

Many authors have tried to circumvent the loss of feedback energy by developing different methods of implementing feedback in SPH type codes. Navarro & White (1993) and Mihos & Hernquist (1994) examined returning part of the energy as a direct velocity "kick" to nearby particles. Gerritsen (1997) and Mori et al. (1997) returned all energy to a single particle which was then artificially inhibited from cooling. Similarly Thacker & Couchman (2000) modified the cooling properties of the particle receiving supernova energy, but they did so by defining a plausible cooling density for the unresolved hot bubble. A completely different approach was taken by Springel (2000), who introduced a separate variable to track the turbulent energy induced by feedback which was then returned slowly to internal energy of the particle. A different approach still is to forsake any pretention of resolving feedback and formulate a complete sub-grid model for the multiphase medium, where supernova feedback is taken into account deriving an effective equation of state for the gas (Springel & Hernquist 2003).

We will not give a complete overview of the different strengths and weaknesses of these methods. For a solid discussion of SPH feedback methods see Thacker & Couchman (2000) and Kay et al. (2002). A recurrent problem for the explicit feedback methods is that it is difficult to get unambiguous control over the strength of the feedback: either physically motivated values of the feedback efficiency give too strong feedback and a laborious and subjective search must be made for an acceptable value or the method gives too weak feedback and energy losses must be limited by an ad hoc intervention. On the other hand, the methods that try to account for feedback implicitly as either an extra reservoir of energy or in a sub-grid model suffer from the problem that it may be impossible to reproduce the effect of feedback on the distribution of gas, that is the occurrence of superbubbles and other phenomena related to the “frothy” ISM.

Here we will present and test two new methods for feedback in SPH codes that address some of the problems of previous feedback implementations.

3.2 Smoothed particle hydrodynamics

Different variants of SPH were tested recently for their ability to model feedback by Springel & Hernquist (2002). They formulated a new SPH scheme that conserves both energy and entropy, contrary to previous formulations and for this reason it turned out to be the most suitable for the implementation of feedback. We will also use this scheme. So we have the standard SPH estimate for the density ρ_i due to a distribution of particles with positions r_i using a kernel function W,

$$\rho_i = \sum_j m_j W(|r_i - r_j|, h_i), \tag{1}$$

where m_i is the mass of particle, h_i its smoothing length and for $W(r,h)$ we take the spline kernel of Monaghan & Lattanzio (1985). The Springel & Hernquist (2002) conservative SPH scheme gives the following equation of motion for the SPH particles,

$$\frac{dv_i}{dt} = -\sum_{j=1}^{N} m_j \left\{ f_i \frac{P_i}{\rho_i^2} \nabla_i W_{ij}(h_i) + f_j \frac{P_j}{\rho_j^2} \nabla_i W_{ij}(h_j) + \Pi_{ij} \nabla \bar{W}_{ij} \right\} \tag{2}$$

with particle velocities v_i, pressures P_i and the f_i defined by:

$$f_i = \left(1 + \frac{h_i}{3\rho_i} \frac{\partial \rho_i}{\partial h_i}\right)^{-1} \tag{3}$$

Here, $\bar{W}_{ij} = (W_{ij}(h_i) + W_{ij}(h_j))/2$ is a symmetrized form of the kernel. For the artificial viscosity tensor Π_{ij} we can take any one of the standard forms (Monaghan

1992, Hernquist & Katz 1989), we will use

$$\Pi_{ij} = \frac{-\alpha\mu_{ij}\bar{c}_{ij} + \beta\mu_{ij}^2}{\bar{\rho}_{ij}}, \tag{4}$$

where

$$\mu_{ij} = \begin{cases} \frac{v_{ij}\cdot r_{ij}}{h_{ij}(r_{ij}^2/h_{ij}^2+\eta^2)} & \text{for } v_{ij}\cdot r_{ij} < 0, \\ 0 & \text{for } v_{ij}\cdot r_{ij} \geq 0. \end{cases}$$

Here $v_{ij} = v_i - v_j$ and $r_{ij} = r_i - r_j$, α, and β are constants of order 1 ($\alpha = 0.5$, $\beta = 1$), η is a parameter to prevent numerical divergences and quantities overlaid with a bar are symmetrized, e.g. $\bar{c}_{ij} = (c_i + c_j)/2$ for the average sound speed of particles i and j.

It is convenient to use the entropic function, defined by $P = A\rho^\gamma$, with γ (=5/3) the adiabatic index of the gas, to track the thermal evolution of the gas, integrating A_i according to

$$\frac{dA_i}{dt} = -\frac{\gamma-1}{\rho_i^\gamma}(\Gamma - \Lambda) + \frac{1}{2}\frac{\gamma-1}{\rho_i^{\gamma-1}}\sum_{j=1}^{N} m_j\Pi_{ij}v_{ij}\cdot\nabla_i\bar{W}_{ij} \tag{5}$$

Here, Γ and Λ represent the external heating and cooling terms. These are determined by consideration of the physical processes that we want to include to model the ISM (see Chapter 2).

3.3 Supernova feedback methods

Here we will examine two new methods to implement feedback in SPH simulations. The first is a variant of the kinetic energy feedback, but imparting random in stead of radial velocity kicks. The second is related to the idea of Gerritsen (1997) of giving one particle all the mechanical energy. We will compare both methods to "normal" particle heating.

3.3.1 Particle heating

As we have argued above simply considering the mechanical energy as a heating term is not a good method of modelling feedback in simulations of galaxies. On the other hand it has been shown by Springel & Hernquist (2002) to represent point explosions well. As such we will consider single particle (SP) heating here for comparison to the more elaborate methods.

We will add all energy e_{sn} that is to be injected into the gas, to the nearest gas particle, changing its entropy by:

$$\Delta A_i = \frac{e_{sn}}{m_i}\frac{\gamma-1}{\rho^{\gamma-1}} \tag{6}$$

There are different ways of applying particle heating (see also the discussion in Thacker & Couchman 2000). One could add a heating term proportional to the local mechanical luminosity to Γ in equation (5) or add the energy produced per time step directly to the thermal energy of neighbouring gas particles. Another method is simply letting every star formation event be accompanied by an injection of an instantaneous energy burst corresponding to all mechanical energy released over time by the mass of stars formed. These methods are very similar but they are expected to behave differently, for the following reasons: 1) the cooling curve has a strong peak so that in case of heating the feedback will be constrained by the peak value of the cooling, whereas an instantaneous thermal energy jump may bypass this peak; 2) in general the local time step is shorter by one or more orders of magnitude than the release time of the supernova energy (typically in the order of 3×10^7 yr). The various methods are described elsewhere (see e.g. Thacker & Couchman 2000) and we will not examine all of these methods. The general conclusion, that thermal energy feedback is not an efficient mechanism, is in all cases not altered.

3.3.2 Kinetic energy feedback

The alternative of adding the SN energy as kinetic energy by modifying the velocities of nearby particles was examined by Navarro & White (1993) and Gerritsen (1997). They found that imparting a radial velocity kick to particles in the neighbourhood of a SN particle results in strong feedback effects. Their conclusion was that, unless a very small fraction (≈ 0.0001) of the original SN energy was used for the velocity kick, the effects of feedback on the ISM would be too strong. This fraction differs substantially from the physically motivated value of ≈ 0.1 for the efficiency of the conversion of supernova energy to kinetic energy of the ISM.

However, we will examine an implementation of kinetic energy feedback (KF) that imparts velocity kicks to neighbouring SPH particles in random directions, as opposed to radial. This is based on the following basic observation about kinetic energy $\mathrm{E_k}$ in SPH, using the SPH identity $\sum_j \frac{m_j}{\rho_j} W_{ij} \approx 1$:

$$
\begin{aligned}
\mathrm{E_k} &= \sum_i \frac{1}{2} m_i v_i^2 \\
&\approx \sum_{i,j} \frac{1}{2} \frac{m_i m_j}{\rho_j} v_i^2 W_{ij} \\
&= \sum_j \frac{1}{2} m_j \sum_i \frac{m_i}{\rho_j} \left\{ (v_i - \bar{v}_i) + 2 v_i \bar{v}_i - \bar{v}_i^2 \right\} W_{ij} \\
&= \sum_j \frac{1}{2} m_j \sigma_i^2 + \sum_j \frac{1}{2} m_j \bar{v}_i^2 \\
&= \mathrm{E_{random}} + \mathrm{E_{bulk}}
\end{aligned} \tag{7}
$$

with $\bar{v}_i$ and σ_i the usual SPH estimates of the local velocity and velocity dispersion. The total kinetic energy of the particles in the simulation can be split (approximately) into a part $\mathrm{E_{bulk}}$, associated with bulk motions of the gas and a part $\mathrm{E_{random}}$ associated with random motions. The random kinetic energy will decrease, even in the absence of bulk motions, because of the coupling to the thermal energy through the effect of the artificial viscosity,

$$\dot{E}_{random} = \sum_{i,j} m_i v_{ij} \cdot \Pi_{ij} \nabla \bar{W}_{ij} \tag{8}$$

and thus it will decay over time and be added to the internal energy of the particles. So by imparting particles with a random velocity we act in fact on a reservoir of energy in between thermal and bulk movements of the gas (one may want to interpret this as the smallest scale of turbulence in the simulation, however it is not entirely clear whether this is justified, numerical tests of relaxing random particle distributions suggest that the decay of kinetic energy (8) happens on timescales, scaled to physical units relevant to our simulation, of $\approx 10^6$ yr). As a result of feedback the velocity dispersion will be enhanced locally. The enhanced velocity dispersion acts as a pressure that can push out surrounding gas with lower dispersion and thus can still result in radial motions and superbubbles.

To be specific, the method consists of giving particles in the neighbourhood of SN particles a random velocity kick with mean magnitude:

$$\Delta v = \sqrt{2 e_{sn} \Delta t W} \tag{9}$$

Note that the $\sqrt{\Delta t}$ dependence guarantees that the feedback does not depend on the size of the local time step. A possible shortcoming of this method is that momentum is not strictly conserved, locally we expect statistical variations due to the limited number of neighbours. It is not difficult to correct for these variations by imposing momentum conservation.

3.3.3 Pressure particle feedback

The mass of hot gas in SN remnants and hot bubbles is generally a small fraction of the total mass of the associated star formation event. The problem of feedback is thus in essence a resolution problem: we form stars at the minimum mass resolution, thus the hot gas mass is much too low to be resolved. Inspired by the fact that the mass of hot gas is very small and by previous feedback implementations that used single hot particles, we propose to model the feedback by considering the zero mass limit of an SPH particle, such that the product $m \times P$ of particle mass and pressure remains constant taking the limit $m \to 0$. We will call such a particle a *pressure particle* (PP) (the connection between our pressure particles and those of Gerritsen will be explained shortly). Such pressure particles will be associated with every new star particle formed in the simulation. The contribution of a pressure particle to the acceleration of neighbouring (normal) SPH particles will be given by taking the limit $m_{PP} \to 0$ of the ordinary expression for the SPH equations of motion, so for example in case of the conservative SPH formulation (from Eq.2):

$$\begin{aligned} \left.\frac{dv_i}{dt}\right|_{PP} &= m_{PP}\Big(f_{PP}\frac{P_{PP}}{\rho_{PP}^2}\nabla W(h_{PP}) + f_i\frac{P_i}{\rho_i^2}\nabla W(h_i) + \Pi\nabla\bar{W}\Big) \\ &\to A_{PP}\rho^{\gamma-2}\nabla W(h_i), \quad \text{as } m_{PP} \to 0. \end{aligned} \tag{10}$$

Here, $A_{PP} = P_{PP}/\rho_{PP}^{\gamma} = (\gamma - 1)e_{PP}/\rho_{PP}^{\gamma-1}$ is the entropic function of the pressure particle. The artificial viscosity term of the SPH equations does not contribute to the

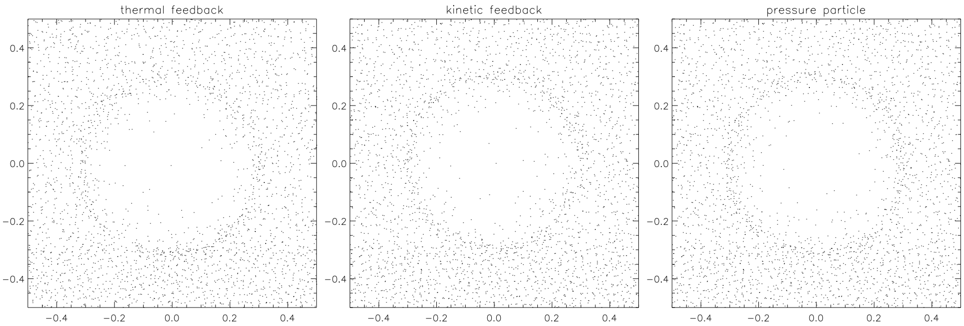

Figure 3.1: Cuts through the particle distribution for the point explosion test. Plotted are the particles closer than 0.05 to the equatorial plane. Each panel shows the results for different feedback method (from left to right: thermal, kinetic and pressure particle feedback).

acceleration as $m_{PP}\Pi_{iPP} \rightarrow 0$ for $m_{PP} \rightarrow 0$. The acceleration of the particle itself will formally diverge in the limit, but we fix the pressure particles to star particles. As a result we lose momentum, in reality this momentum would be carried by the hot gas "pushing" against the surrounding gas, and it would be returned to the ISM at some point. We correct for this by assigning all momentum to the particle in the neighbourhood of the pressure particle that is most "antipodal" to the direction of the lost momentum (This also ensures to first order angular momentum conservation). The entropy A_{PP} is the variable that determines the strength of feedback, and its evolution in time is an input to the model that depends on the amount of star formation but also on assumptions about energy loss and remnant evolution that are not resolved in the code. It is acceptable to fix this as an input model, as we had determined that we cannot in any way follow realistically the evolution of SN remnants. Here we will use relatively simple prescriptions for A_{PP} (which we will describe below); in principle one could invoke results of more detailed models/ simulations in its evolution. Note that the method is in some ways similar to the approaches of Gerritsen (1997) and of Tacker & Couchman (2000), in that the feedback is effected by one particle, but rather than just fixing and preventing an ordinary SPH particle from cooling (Gerritsen) or defining an effective density (Tacker & Couchman) we choose to explicitly treat SN particles as separate entities. The advantage of our approach is that we have a well defined model (namely the prescription for A_{PP}) which we can vary according to our assumptions for the unresolved physics. Furthermore, it is numerically well behaved and does not suffer from the numerical instabilities that can occur in Gerritsen's method (Bottema 2002, priv. comm.).

3.4 Sedov blast wave test

In order to assess the capabilities of the various feedback schemes to model explosive events we test the ability of the methods to model a point explosion in a background of constant density and zero thermal energy. In this test we do not use cooling. This test is described in Springel and Hernquist (2002) for single particle heating. They found that, for the conservative SPH formulation, SPH reproduces the speed of the

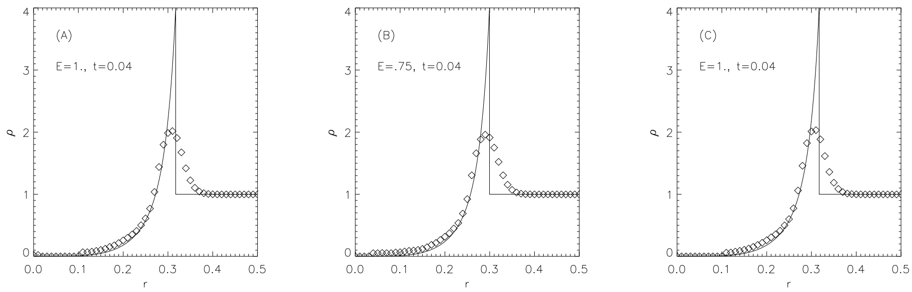

Figure 3.2: Radial density profiles for the point explosion test. A: thermal feedback, B: kinetic feedback C: pressure particle feedback. Diamonds indicate the spherically averaged density for a $\mathrm{N} = 64000$ run. The analytical solution follows the drawn line.

shock front and the shape of the inner density profile of the analytic solution (e.g. Landau & Lifschitz 1987). The density contrast at the shock location is generally too low at moderate resolution due to the smoothing properties of the SPH kernel estimate for the density. Also visible in the particle plots of Springel & Hernquist (their Figure 2) are some artifacts due to the use of a regular grid as the initial particle distribution. The solution for this problem is the use of initial conditions without preferred directions (Thacker & Couchman 2000). This is not really a restriction as this is also the case for the typical particle distributions that are present in the course of a simulation. For the test we therefore used as the initial particle distribution a glass state: a smooth gas box of consisting of an SPH particles relaxed from a Poisson distribution. Drawback of this approach is that the density exhibits variations of order $\delta\rho/\langle\rho\rangle \sim 0.01$ (which is much smaller than the scatter in density of the non-relaxed initial condition, ~ 0.1). We show results for $\mathrm{N} = 64000$, results for other resolutions are similar and consistent with the resolution study in Springel and Hernquist (2002). The mean density is set to $\langle\rho\rangle = 1$, the temperature of the gas is set at the minimum allowed. At the start of the simulation a point explosion with energy $\mathrm{E} = 1$ is set off at the origin, implemented in accordance with the respective feedback methods. For SP feedback this means that at $\mathrm{t} = 0$ all energy is put into one particle in the centre of the box. For the KF method an instantaneous random velocity kick is given in the centre of the gas distribution according to Eq. 9. For PP feedback a pressure particle with $\mathrm{A} = 2/3$ is placed at the origin. The pressure particle is evolved adiabatically so A (the entropy) stays constant.

In Fig. 3.1 we plot the particle distributions after $\mathrm{t} = 0.04$ for all three methods while in Fig. 3.2 we have plotted the radial density distributions. If we compare these to Fig. 2-4 in Springel & Hernquist (2002) we see that the particle distributions show slight deviations from spherical symmetry. This is due to the fact we have started from initial conditions with small perturbations. Otherwise the results are qualitatively the same. Note especially that for KF there is no remnant visible from the initial anisotropic velocity kicks. All three methods show very similar behaviour, and are certainly equivalent. We conclude that all three methods considered here can be used to model point explosions, and so are in principle good candidates for use as supernova feedback models in galaxies.

3.5 Feedback in dwarf galaxies

Next we will test our feedback prescriptions in a realistic model for a dwarf irregular (dIrr) galaxy. These dwarf galaxies are ideal feedback "labs." Free from the effects of differential rotation and spiral density waves the prime regulator of star formation activity is probably the energy input by young stars (Hunter 1997). Thus the outcome of the modelling will be sensitive to the quality of the feedback implementation. We will test our feedback methods implemented in a code that has a realistic model for ISM and star formation.

dIrrs are a well studied group of galaxies: HI observations show that their ISM is heavily perturbed: their HI distribution is dominated by holes, shells and filaments, giving a frothy structure (e.g. Walter 1999, Stil 2002b). The velocity dispersions of HI in dwarf galaxies are generally in the order 10 km/s and some stirring force is needed to maintain this velocity dispersion against dissipation (Stil 2002a), SN explosions being one of the candidates. The challenge then is to have a feedback scheme that manages to reproduce a dwarf galaxy with a dynamic ISM, whose star formation properties and ISM structure are constrained by these observations.

3.5.1 ISM and star formation model

For the ISM model we use the model D of Chapter 2 for a subsolar metallicity of $\mathrm{Z} = \mathrm{Z}_{\odot}/5$. This model is a comprehensive model for the neutral ISM and it includes realistic cooling as well as heating by UV light from stars, including the effects of grain charging, and it solves the ionization balance including cosmic ray ionizations. For the primary cosmic ray ionization rate we take $\zeta_{\mathrm{CR}} = 3.6 \times 10^{-17}\ \mathrm{s}^{-1}$.

The most important feature of the ISM model is that it allows to follow cooling and collapse of the warm neutral medium (WNM) to the cold neutral medium (CNM): warm, partially ionized gas (with temperatures $\mathrm{T} = 10^4$ K and ionization fraction $\mathrm{x_e} \approx 0.1$) that is stable with respect to gravitational collapse, will cool down as soon as heating of the gas decreases (due to for example a decrease in UV irradiation as nearby stellar populations age). As a region cools down and loses its pressure support collapses it will become eligible to form stars.

Our star formation recipe is similar to that used by Gerritsen & Icke (1997), and is amply discussed in Chapter 2. In short it considers a particle unstable to star formation if the local Jeans mass $\mathrm{M_J}$ is smaller than a reference mass $\mathrm{M_{ref}}$,

$$\mathrm{M_J} = \frac{\pi\rho_\mathrm{i}}{6}\left(\frac{\pi \mathrm{c_i^2}}{\mathrm{G}\rho_\mathrm{i}}\right)^{3/2} < \mathrm{M_{ref}}. \tag{11}$$

The reference mass $\mathrm{M_{ref}}$ is chosen such that it is approximately equal to the smallest resolvable mass. If a particle is unstable to star formation it will form stars on a timescale τ_{sf} that scales with the free-fall timescale τ_{ff},

$$\tau_{\mathrm{sf}} = \mathrm{f_{sf}} \mathrm{t_{ff}} = \frac{\mathrm{f_{sf}}}{\sqrt{4\pi \mathrm{G}\rho}}. \tag{12}$$

Here, $\mathrm{f_{sf}}$ is a delay factor that accounts for the fact collapse is delayed by either turbulence or magnetic fields (Mac Low & Klessen 2004, Shu et al. 1987).

The stellar particles that are formed carry an age. We use Bruzual & Charlot (1993) models for a Salpeter IMF to calculate UV luminosities (in the range $912 - 2100$ Å) needed for the calculation of the local radiation field.

3.5.2 Initial conditions

We construct initial conditions by constructing a model for a dwarf galaxy consisting of 3 components: gaseous disk, stellar disk and a dark halo. In the simulations presented here the dark halo is taken to be a fixed background potential with a density profile

$$\rho(r) = \rho_0 \frac{e^{-r^2/R_{ct}^2}}{r^2 + r_c^2}, \tag{13}$$

with central density of $\rho_0 = 0.02\ \mathrm{M_\odot}$ pc^{-3}, cutoff radius $\mathrm{R_{ct}} = 20$ kpc and core radius $\mathrm{r_c} = 2$ kpc. This halo profile is chosen rather than the Navarro, Frenk & White profile we used in Chapter 2 because the halos of dwarf galaxies are seen to have flat density cores (Burkert 1995). For the stellar component we construct an exponential disk,

$$\rho_{\mathrm{disk}}(\mathrm{R}, \mathrm{z}) = \frac{\Sigma_0}{2\mathrm{h_z}} \exp(-\mathrm{R}/\mathrm{R_d}) \mathrm{sech}^2(\mathrm{z}/\mathrm{h_z}) \tag{14}$$

with central surface density $\Sigma_0 = 300\ \mathrm{M_\odot}$/pc^2, radial scale length $\mathrm{R_d} = 0.5$ kpc and vertical scale height $\mathrm{h_z} = 200$ pc. So the total stellar mass is $1.5 \times 10^8\ \mathrm{M_\odot}$. It is constructed using the approximation of a three integral distribution function of Kuijken & Dubinski (1995). The stellar particles are initialised randomly with ages of up to 12 Gyr old. The gas disk is constructed with a radial surface density profile,

$$\Sigma = \frac{\Sigma_\mathrm{g}}{1 + \mathrm{R}/\mathrm{R_g}}, \tag{15}$$

with central density $\Sigma_\mathrm{g} = 8\ \mathrm{M_\odot}$/pc^2 and radial scale $\mathrm{R_g} = 0.5$ kpc, truncated at 6 kpc, for a total mass of $10^8\ \mathrm{M_\odot}$. Initially the gas disk is given a temperature of 8000 K.

3.5.3 The mechanical luminosity

The stellar particles that are formed in the simulation do not represent single stars but have masses in the order of a few hundred to few thousand solar masses. They can be considered to be stellar clusters, and we will assume that stars in these clusters are formed with masses distributed according to a Salpeter IMF, $\Phi \propto \mathrm{M}^{-1.35}$ with lower cutoff mass $\mathrm{M_{low}} = 0.1\ \mathrm{M_\odot}$ and upper cutoff $\mathrm{M_{upper}} = 100\ \mathrm{M_\odot}$. Gerritsen & Icke (1997) discussed the effect of other choices for the IMF, they found that because the amount of mechanical energy produced by a cluster depends sensitively on the shape of the IMF, the results with respect to star formation are sensitive to this choice. Note that this uncertainty is often encountered in astrophysical studies related to star formation, and, in the context of a self regulated model for star formation translates to an uncertainty in the exact star formation rates. The masses of the "star clusters" that are formed, are small enough that formally the number of heavy stars, and hence the mechanical luminosity, should vary from particle to particle due to sampling effects.

In practice we will still assume a complete sampling of the IMF even for low mass particles. At least this yields a reasonable estimate for the mechanical luminosity. The possible impact of this assumption is further reduced by the fact that a star forming region will in general produce multiple star particles, which increases the effective cluster size.

Given the distribution of initial masses of stars the mechanical luminosity can be derived from stellar evolution models. The following provides an estimate of this luminosity that is good enough for our purposes:

$$\mathbb{L}_{\mathrm{mech}} = \frac{\mathrm{n_{sn}E_{sn}}}{\Delta \mathrm{t_{sn}}} \text{ erg s}^{-1} \mathrm{M_\odot}^{-1}. \tag{16}$$

Here, $\mathrm{n_{sn}} = 0.009 \mathrm{\ M_\odot}^{-1}$ is the number of supernova per solar mass of stars formed. This number is derived for our IMF assuming all stars with masses above $\mathrm{M} = 8 \mathrm{\ M_\odot}$ explode as type II supernovae. These supernovae yield an energy $\mathrm{E_{sn}} \approx 10^{51}$ erg, and while stellar winds can contribute significantly in the first few Myr, type II SNe constitute the bulk of the energy input. An active period of $\Delta \mathrm{t_{sn}} = 30$ Myr (approximately the lifetime of an $8 \mathrm{\ M_\odot}$ star), during which the mechanical luminosity is assumed constant, is adopted. In Chapter 2 (Fig. 2.11) we have plotted this prescription compared to a more detailed model.

For the SP and KF feedback methods the mechanical luminosity can be used directly as the amount of heat or kinetic energy to be injected into the ISM. However for the PP method we need to specify additionally the thermal evolution of the supernova particle. Here we evolve the entropy $\mathrm{A_{PP}}$ according to

$$\frac{\mathrm{dA_{PP}}}{\mathrm{dt}} = \frac{\gamma - 1}{\rho^{\gamma-1}} \epsilon_{\mathrm{PP}} \mathrm{m}_\star \mathbb{L}_{\mathrm{mech}}, \tag{17}$$

where $\rho = \rho(\mathrm{r_{PP}})$ is the density at the PP location, ϵ_{PP} the efficiency of PP feedback and $\mathrm{m}_\star$ the mass of the new stellar particle. After $\Delta \mathrm{t_{sn}}$ we assume that the hot gas in the bubble will quickly cool, and thus we set $\mathrm{A_{PP}} = 0$ and remove the pressure particle from the calculation. For the efficiency parameter we will assume that 90% of the available energy is radiated away (in structures we cannot resolve), thus $\epsilon_{\mathrm{PP}} = 0.1$. This value comes from more detailed simulations of the effect of supernova and stellar winds on the ISM (Silich et al. 1996), and is also used in other simulations of galaxy evolution (e.g. Semelin & Combes 2002, Springel & Hernquist 2002, Buonomo et al. 2000). A similar thermal evolution of SN remnants was shown by Oey & Clarke (1997) to be consistent with the size distribution of superbubbles in the Small Magellanic Cloud and Holmberg II.

Note that the constancy of the efficiency ϵ may not be valid. It may depend on the environment of the star formation location. In that case it may be worthwhile, especially for application of the model to extreme conditions (like dense cores in mergers, or formation of central clusters in galaxies), to explore this parameter further.

3.5.4 Feedback test runs

In addition to the three different methods for feedback we will let our model galaxy run without any SN feedback, letting the gas only experience heating by UV light of young stars. Thus we run 4 different runs indicated by their feedback method: FUV for the UV feedback only run, in addition to SP, KF and PP feedback runs.

In all simulations we use the full ISM and star formation model, the only difference between them being the feedback method. We will run simulations at low (20k gas particles and 20k star particles) and high resolution (200k resp. 200k). We stop the runs at approximately 1 Gyr, at which point any transient features from the initial conditions are gone.

3.5.5 Results

In Fig. 3.3 we show cuts through the central plane of the resulting galaxies at the end of the simulation showing density and temperature for the low resolution runs, while in Fig. 3.4 we have shown corresponding plots for the high resolution runs. If we look at the FUV runs first, we see that the ISM in these stay in a rather cold state at 20k resolution. The inner 2 kpc of the galaxy has a temperature $T \lesssim 1000$ K. For high resolution the disks collapses in dense clumps or stretched filaments, due to these the density distribution looks highly structured with many spiral arms. For the SP run we see that supernova feedback manages to create very small warm bubbles of $T = 10^4$ K. However the density distribution is still very structured.

The density distribution of the KF and PP are qualitatively very similar and show a density distribution with large voids (< 1 kpc big) caused by feedback. Note that area of the disk where star formation can happen is actually larger in case of the KF and PP runs than in FUV and SP runs. If we look at the the temperatures in case of PP feedback we see that they reach much higher values in those bubbles, this is due to the fact that in case of KF the energy is put into random motions of the gas, while the maps for PP feedback show the hotspots where pressure particles contribute to temperature. The temperatures in case of PP feedback fall short of the temperature of the gas associated with superbubbles (10^{5-6} K vs 10^{6-7} K). This is caused by the fact that the temperatures are derived using a smoothing procedure: the mass in the hot bubbles is lower than the mass resolution, so cold material contributes to the temperature estimate. As we increase resolution we see that the derived temperatures increase for a bubble of given size as it becomes better resolved. However, the strength of the feedback is not affected, because the strength of the feedback is not determined by this temperature.

Comparing the low and high resolution runs, we see that the high resolution runs show more structure on the small scales, as of course expected, but still high resolution runs are very similar in that there is still a similar number of large shells.

HI: morphology & kinematics

To facilitate comparison with observations, we extract HI data cubes from snapshots of the simulations using the position, velocity, temperature and ionization information of the gas particles. The three dimensional data cube consists of a projection of the 6-dimensional particle distribution in position-velocity on the spatial x-y plane and the z velocity axes, with particles smoothed according to their smoothing lengths in the spatial dimension and according to the Doppler-width corresponding to their temperature in velocity space. It contains the information an observer would be able

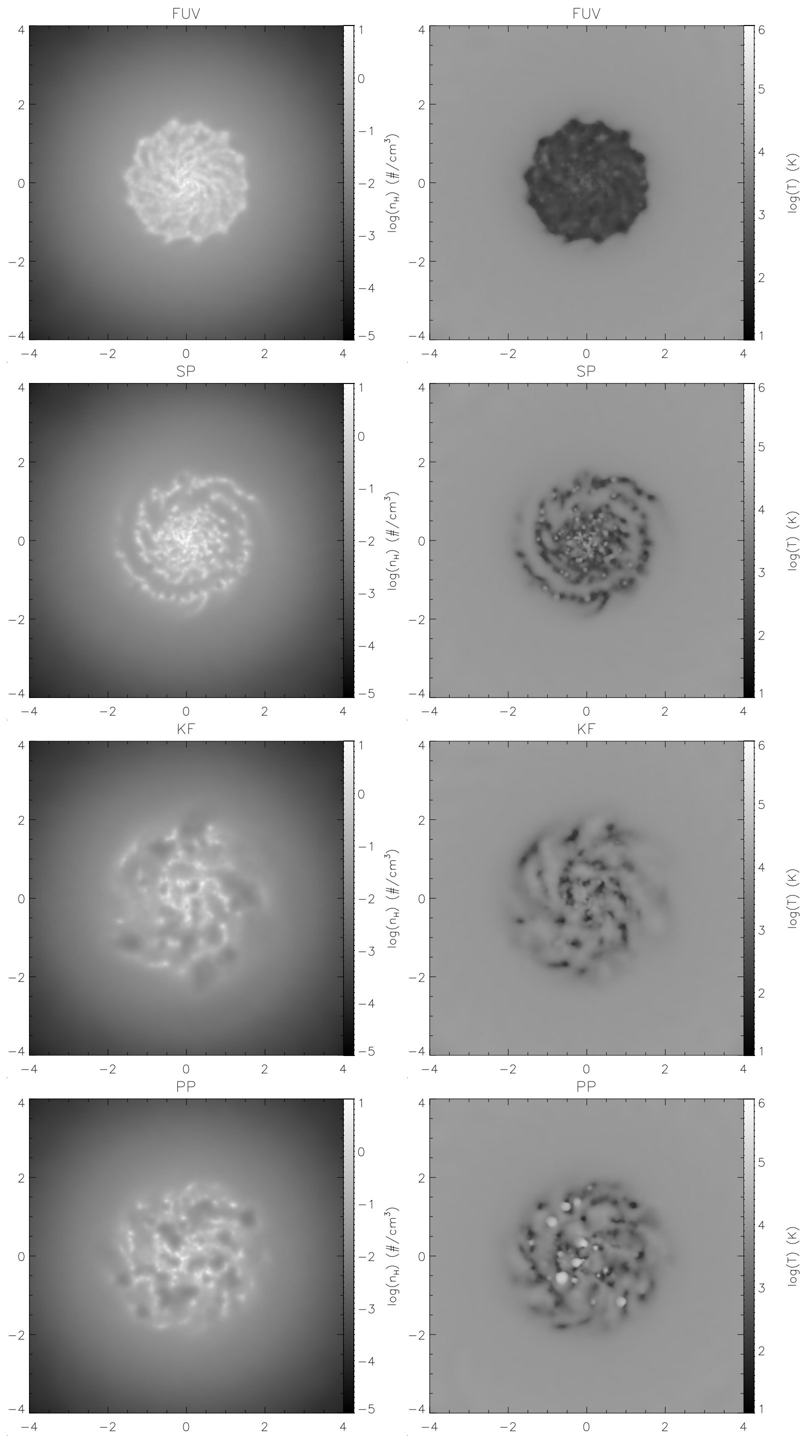

Figure 3.3: Density and temperature of the 20k runs. Shown are cuts through the midplane of H density (left panels) and temperature (right panels). Axes give image scale in kpc.

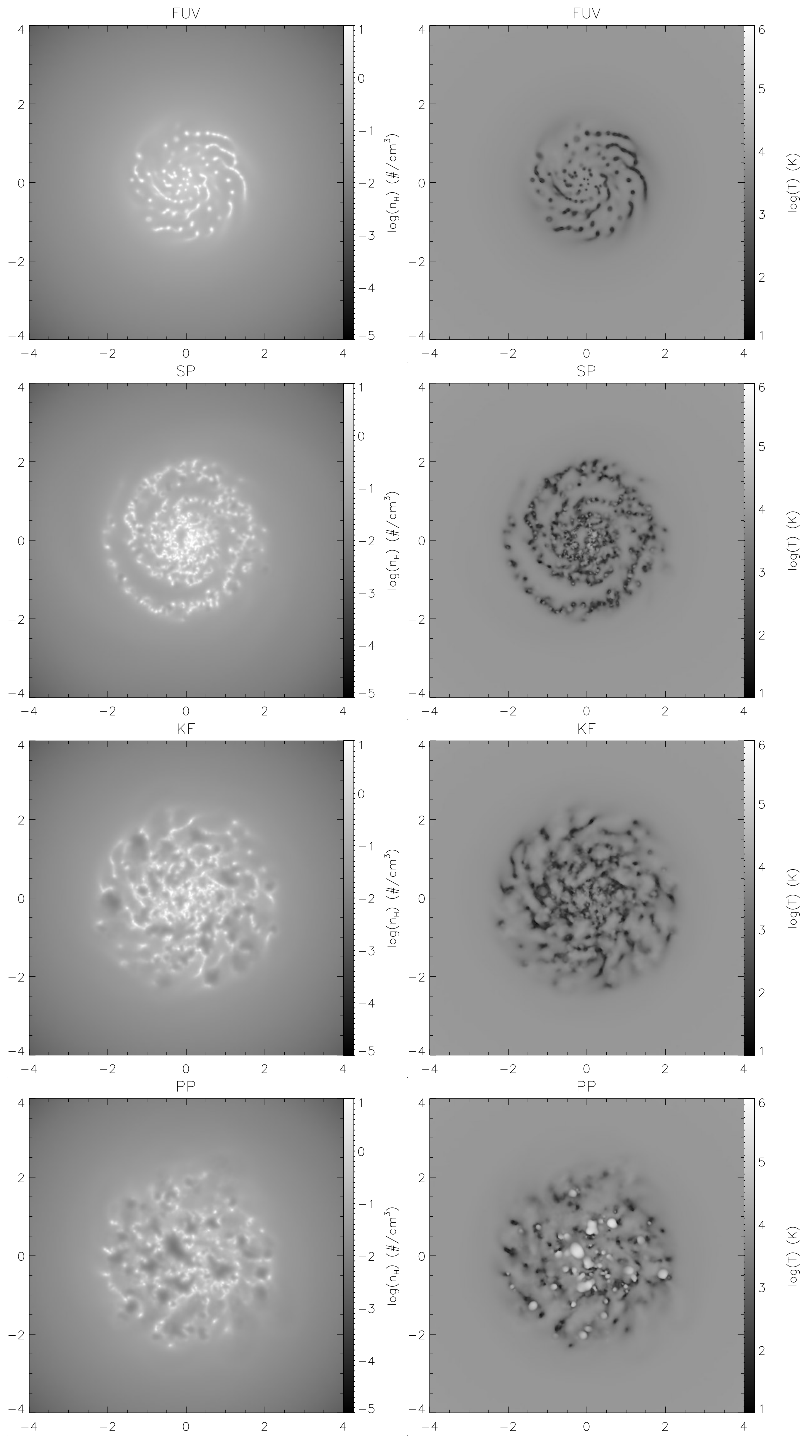

Figure 3.4: Density and temperature of the 200k runs. Shown are cuts through the midplane of H density (left panels) and temperature (right panels). Axes give image scale in kpc.

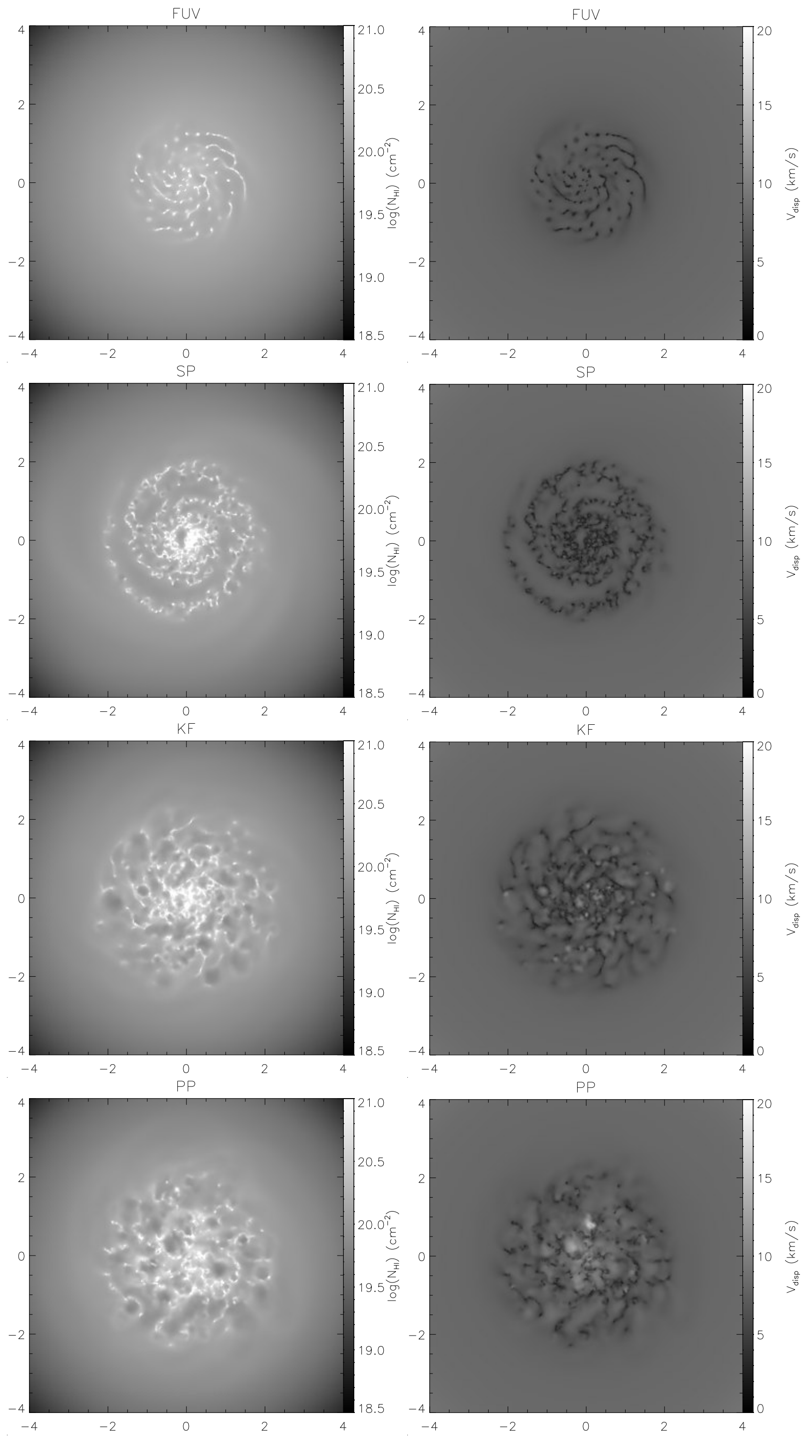

Figure 3.5: HI column density (left panels) and velocity dispersion (right panels) maps of the 200k runs. Axes give image scale in kpc.

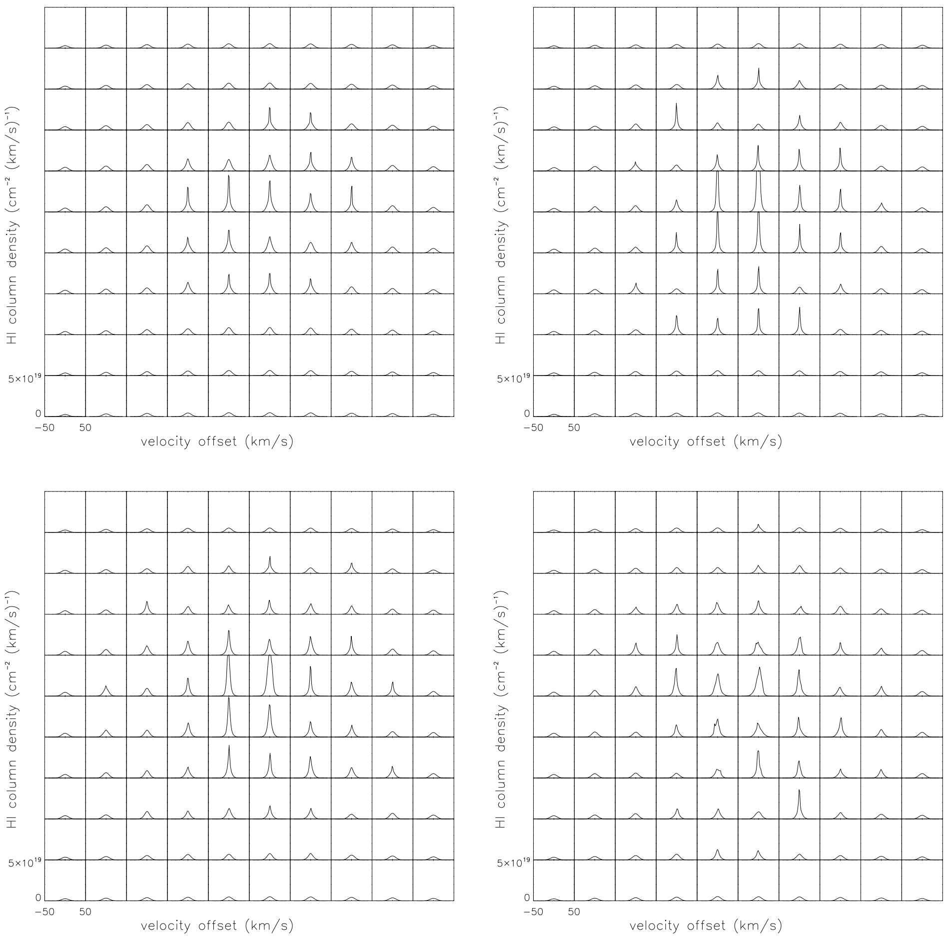

Figure 3.6: HI line profiles, averaged over 200×200 pc regions. **top left:** FUV, **top right:** SP, **bottom left:** KF, **bottom right:** PP.

to extract from face-on observation of the model galaxy (however, no noise or instrumental effects are added, so it is not a real synthetic observation). In Fig. 3.5 we map HI column density and velocity dispersion of our simulated data cubes, while in Fig. 3.6 we have plotted line profiles extracted from them. If we compare these HI maps to observations we see that the FUV feedback shows a regular spiral structure that is generally not observed in dIrr. SP feedback gives a more realistic HI map, but there is still large coherent spiral structure visible. KF and PP feedback give more chaotic and realistic appearance.

We can try to confirm this subjective impression by examining power spectra of the HI maps. Analysis of the power spectra was done recently for a high resolution map of the Large Magellanic Cloud (LMC) by Elmegreen et al. (2001). The LMC is an ideal system for this comparison, as it is the dIrr that can be studied in most

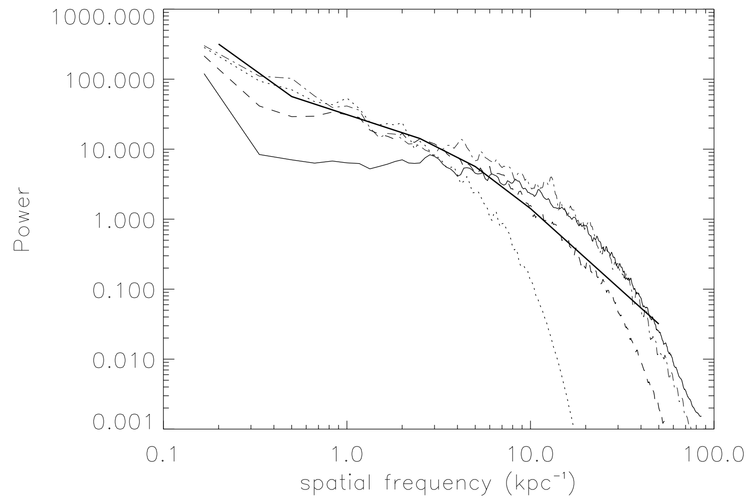

Figure 3.7: Power spectra of HI. Plotted are the power spectra obtained from averaging the 1-dimensional power spectra from the pixel lines of HI maps of simulated HI maps or an HI map of the LMC (Kim et al. 1998). *Thick drawn line:* power spectrum of the LMC (Elmegreen et al. 2001), the other spectra are from HI maps of the simulations (KF is omitted for clarity, it is very similar to PP): *thin drawn line:* FUV (200k), *dash-dotted:* SP (200k), *dotted:* PP (20k) and *dashed:* PP (200k). The scale of the power is arbitrary, but the same for all simulation spectra, for the LMC data it has been scaled to match the PP spectrum between 1 and 10 kpc^{-1}.

detail. For the central 6×6 kpc of our HI maps, we construct 1024$\times$1024 maps (such that the sampling scale is clearly smaller than the smallest resolved structures of the simulation, which are about 20 pc in size). Subsequently we calculate power spectra by summing the 1-dimensional power spectra obtained from the HI map pixel rows. As has been discussed in Elmegreen (2001) this procedure yields information about the contribution of structures at different scales to the HI distribution: the scale-free power law spectra of the LMC (and similar analysis for the SMC and other galaxies) have been interpreted as evidence for a fractal gas distribution. Fig. 3.7 shows the spectra of the simulations together with the spectrum from the LMC (data of this plot is taken from figure 3 of Elmegreen et al. 2001). The spectrum of the PP (and also KF) simulation is remarkably similar to the LMC, and fits much better than either FUV or SP. The FUV simulation shows a lack of power at kpc scales compared to simulations with feedback and the LMC map. This suggests that *energy input from stars is important for structure at kpc scales,* and that gravity and the thermal instability act on smaller scales. Note that the PP spectrum deviates (as do the other feedback methods) at large frequencies because of a steep drop in power at small scales. This is due to the resolution limits of our simulation: the low resolution simulation correspondingly falls off sooner, while giving roughly the same spectrum at large scales.

In the dispersion maps (Fig. 3.5) we can see the presence of gas of low and high dispersion. The WNM has an thermal velocity dispersion of $8 - 10$ km/s, the CNM of 1 km/s. The minimum velocity dispersion of the cold gas is about 3 km/s and is the same for all simulations. Dispersion above 10 km/s are only present in the KF and PP simulations. Note that the correspondence of the dispersion of the cold component of the simulation ($3-5$ km/s) with observed HI velocity dispersions (also in this range) is somewhat fortuitous, because the velocity dispersion which is observed may originate from turbulence at sub cloud scales, that are not resolved in our simulation. Nevertheless the basic picture that comes out of our simulation is realistic: a two component ISM, where lines of sight dominated by the WNM have velocity dispersions in the order of 10 km/s while regions dominated by the CNM have lower velocity dispersions (but higher than the dispersion of 1 km/s corresponding to typical CNM temperatures of 100 K).

Young et al. (2003) studied line profiles of HI observations of a number of dIrrs and derived the presence of two components, one with a velocity dispersion of ≈ 10 km/s, which was present at all locations, and one with a lower dispersion of ≈ 5 km/s with a more patchy distribution. These can be interpreted as being the WNM and a cloud ensemble of CNM clouds. This interpretation is consistent with our simulation. If we look at the line profiles in Fig. 3.6 we see the presence of these two components in the peaked line profiles. Note also that, whereas the profiles of FUV, SP and KF are very regular, PP shows lopsided and irregular profiles, and also double peaks indicative of expanding shells.

HI: relation with star formation

In the literature a number of relations between the properties of the HI distribution and star formation (as traced by Hα) are reported.

Comparing HI surface density and Hα, there seems to be a minimum HI column density below which star formation cannot take place: a threshold column of about $\mathrm{N_{HI}} \approx 3-10\times10^{20}$ cm^{-2} is found if the azimuthally averaged HI and Hα emission are examined as a function of radius (Kennicutt 1989, Hunter et al. 1998), while the threshold also seems to hold locally (Stil 1999). It is not completely clear what the nature of this threshold is, for normal Sc spiral galaxies Kennicutt (1989) showed that it could be understood in terms of critical surface density Σ_c for disk instabilities, $\Sigma_\mathrm{c} = \alpha\kappa\sigma/\pi\mathrm{G}$, with epicyclic frequency κ and dispersion velocity σ. However this criterion seems to fail for dIrr galaxies, even when the value of the constant α is allowed to vary from its value of $\alpha = 0.7$, empirically derived for spiral galaxies (Hunter et al. 1998).

Examining the relation of star formation with HI kinematics a number of authors (Dickey 1990, Young & Lo 1997,1996,Stil 1999, a.o.) found, perhaps somewhat surprisingly, that a positive correlation between local Hα intensity and HI velocity dispersion is *not* observed. As has been extensively discussed by Stil (1999) this is contrary to expectation if supernovae explosions and winds from young stars are the source of mechanical energy in the ISM, thus casting some doubt on young stars as the main stirring agent of the ISM.

We check these findings for the corresponding relations of our models using KF and PP feedback by making projections of the luminosity of stellar particles in ionizing photons (in lieu of Hα) and compare these maps with the HI maps. In Fig. 3.8 we have plotted a scatter diagram of pixel values of the HI maps and "Hα" maps, in Fig. 3.9 the pixel values of the dispersion map and the Hα maps are plotted. We can clearly see that our simulation reproduces the threshold density (Fig. 3.8), albeit at

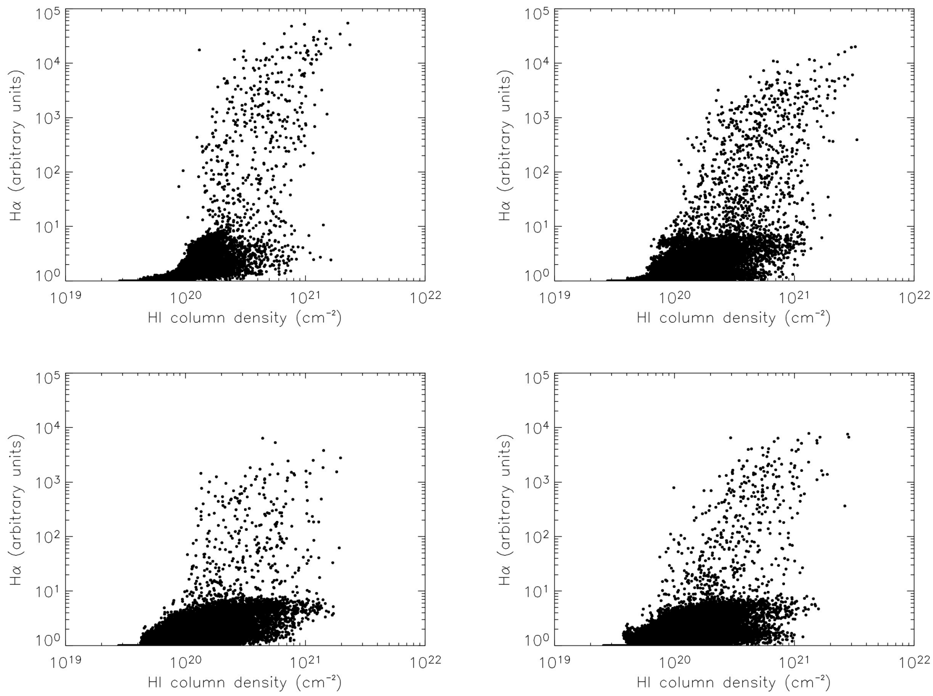

Figure 3.8: HI Column density vs Hα. **top left:** FUV, **top right:** SP, **bottom left:** KF, **bottom right:** PP.

$\mathrm{N} = 1-2\times10^{20}$ cm^{-2}, which is at the low end of the threshold densities reported (e.g. Kennicutt 1989). This shows that in addition to the radial cutoff of star formation, which Gerritsen & Icke showed is natural result of the requirement for cold gas to form in our model, we also reproduce the local threshold. It is purely a result of the ISM model and star formation recipe, as all feedback methods show a similar threshold.

If we look at relation between velocity dispersion and Hα, we see that for the case of FUV and SP feedback Hα emission is seen preferentially at lower dispersion, and only below 7 km/s. Higher dispersions for these feedback methods indicate WNM dominated regions, where star formation cannot take place. For KF and PP feedback high Hα occurs at the whole range of dispersion values, but there is no positive correlation between Hα and velocity dispersion. The reason for this is twofold: 1) Star formation will preferentially occur in quiet regions, where low dispersions allow for large regions of the ISM to collapse (this occurs also in the simulations with inefficient feedback) and 2) the production of ionizing photons by a young stellar cluster occurs mainly in the very beginning of the lifetime of a cluster, and the maximum effect of feedback is delayed with respect to the peak in ionizing luminosity. This is visible in the KF and PP plot as a tendency for Hα values to be higher in low dispersion regions, then as the cluster gets older and less luminous, the HI velocity dispersion increases.

It is remarkable that our simulation reproduces the absence of a strong positive

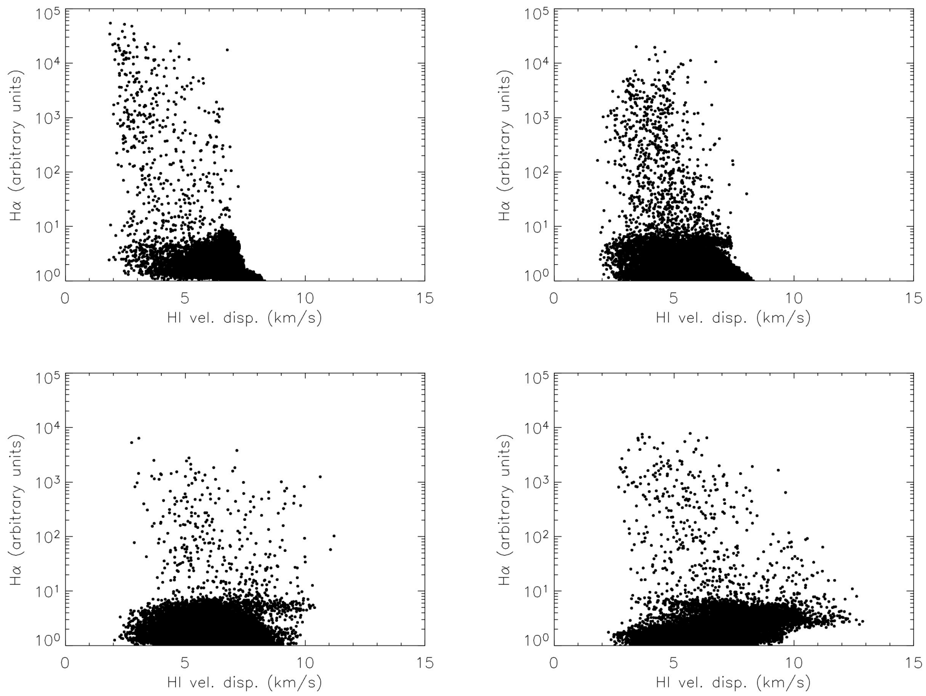

Figure 3.9: HI velocity dispersion vs Hα. **top left:** FUV, **top right:** SP, **bottom left:** KF, **bottom right:** PP.

correlation of velocity dispersion and Hα: we know for sure that the high dispersions in the simulation are caused by feedback. This means that the naive reasoning behind the expectation of a positive correlation is false, and shows the necessity of exploring star formation and feedback in fully dynamic models.

3.6 Conclusions

In this work we have examined two new methods (which we designated the KF and PP method respectively) for implementing feedback in galaxy simulations using SPH. The KF method returns the mechanical energy of young star clusters as a random velocity perturbation. The PP method constructs a *pressure particle*, which is the zero mass limit of an ordinary SPH particle, at the site of new stellar associations. They have been designed specifically to circumvent the loss of feedback energy occurring in normal particle heating. We have checked the results of the new methods against normal energy injection for the Sedov blast wave test. Next we have examined their behaviour in detailed simulations of star formation in dwarf galaxies. Our findings are the following:

- Both the KF and PP feedback method are equivalent to normal particle heating in simple Sedov blast wave tests.

- The morphology and kinematics of simulated dIrr galaxies for the new methods shows holes and shells similar to those observed in dIrr galaxies, while applying no feedback or returning SN energy as thermal energy allows for a sharply defined spiral structure to form.

- Comparison of the power spectra of HI maps of the simulations with LMC observations shows that the KF and PP feedback methods reproduce the spectra obtained from observations, down to the resolution limit of the simulation. Furthermore, comparison of the spectra shows that stellar energy input determines the ISM structure at kiloparsec scales, while structures at smaller scales are determined by gravitational collapse and/ or thermal instability.

- The resulting model galaxies reproduce the observed relations of HI and Hα. An HI threshold for star formation is found, which is the result of the star formation recipe. The new feedback methods are necessary to reproduce the absence of correlation between Hα emission and HI velocity dispersion over the full range of observed velocity dispersions. The surprising fact that the Hα emission and HI velocity dispersion are not correlated is due differences in timing between local stirring of the gas by feedback and the maximum Hα luminosity of young stellar clusters and as a result of the preference of star formation for low dispersion regions.

The fact that the new methods reproduce observed dwarf galaxies in detail, including the general morphology, kinematics, the power law behaviour of the spectra of HI maps and the relations between star formation and velocity dispersion show that feedback is a necessary ingredient, and that the KF and PP methods represent the effects of feedback significantly better than previous methods. Of the two methods we have presented we have a slight preference for the PP method, as this method gives sharper defined structure and higher velocity dispersions. Furthermore it has a well defined input model. An advantage of the KF method is that it is more efficient, allowing for larger time steps (the extra computational costs incurred by the additional work load of feedback routines themselves is in both cases negligible).

References

Buonomo, F., Carraro, G., Chiosi, C., & Lia, C., 2000, *MNRAS* **312**, 371

Burkert, A., 1995, *ApJ* **447**, L25+

Elmegreen, B. G., Kim, S., & Staveley-Smith, L., 2001, *ApJ* **548**, 749

Fragile, P. C., Murray, S. D., Anninos, P., & Lin, D. N. C., 2003, *ApJ* **590**, 778

Gerritsen, J. P. E., 1997, *Ph.D. thesis*, Groningen University

Gerritsen, J. P. E. & Icke, V., 1997, *A&A* **325**, 972

Gingold, R. A. & Monaghan, J. J., 1977, *MNRAS* **181**, 375

Hernquist, L. & Katz, N., 1989, *ApJS* **70**, 419

Hunter, D., 1997, *PASP* **109**, 937

Hunter, D. A., Elmegreen, B. G., & Baker, A. L., 1998, *ApJ* **493**, 595

Katz, N., 1992, *ApJ* **391**, 502

Kay, S. T., Pearce, F. R., Frenk, C. S., & Jenkins, A., 2002, *MNRAS* **330**, 113

Kennicutt, R. C., 1989, *ApJ* **344**, 685

Kennicutt, R. C., 1998, *ApJ* **498**, 541

Kuijken, K. & Dubinski, J., 1995, *MNRAS* **277**, 1341

Landau, L., 1987, *Fluid Mechanics (Course of Theoretical Physics)*, Vol. 6, Butterworth-Heinemann, second edition

Leitherer, C., Schaerer, D., Goldader, J. D., Delgado, R. M. G., Robert, C., Kune, D. F., de Mello, D. F., Devost, D., & Heckman, T. M., 1999, *ApJS* **123**, 3

Lucy, L. B., 1977, *AJ* **82**, 1013

Mac Low, M. & Ferrara, A., 1999, *ApJ* **513**, 142

Mac Low, M. & Klessen, R. S., 2004, *Rev. of Mod. Phys.* **76**, 125

Mihos, J. C. & Hernquist, L., 1994, *ApJ* **437**, 611

Monaghan, J. J., 1992, *ARA&A* **30**, 543

Monaghan, J. J. & Lattanzio, J. C., 1985, *A&A* **149**, 135

Mori, M., Yoshii, Y., Tsujimoto, T., & Nomoto, K., 1997, *ApJ* **478**, L21+

Navarro, J. F. & White, S. D. M., 1993, *MNRAS* **265**, 271

Oey, M. S. & Clarke, C. J., 1997, *MNRAS* **289**, 570

Semelin, B. & Combes, F., 2002, *A&A* **388**, 826

Shu, F. H., Adams, F. C., & Lizano, S., 1987, *ARA&A* **25**, 23

Silich, S. A., Franco, J., Palous, J., & Tenorio-Tagle, G., 1996, *ApJ* **468**, 722

Springel, V., 2000, *MNRAS* **312**, 859

Springel, V. & Hernquist, L., 2002, *MNRAS* **333**, 649

Springel, V. & Hernquist, L., 2003, *MNRAS* **339**, 289

Stil, J. M., 1999, *Ph.D. thesis*, Leiden University

Stil, J. M. & Israel, F. P., 2002a, *A&A* **389**, 29

Stil, J. M. & Israel, F. P., 2002b, *A&A* **389**, 42

Thacker, R. J. & Couchman, H. M. P., 2000, *ApJ* **545**, 728

Walter, F., 1999, *Publications of the Astronomical Society of Australia* **16**, 106

Young, L. M., van Zee, L., Lo, K. Y., Dohm-Palmer, R. C., & Beierle, M. E., 2003, *ApJ* **592**, 111